

RSC Advances



This is an *Accepted Manuscript*, which has been through the Royal Society of Chemistry peer review process and has been accepted for publication.

Accepted Manuscripts are published online shortly after acceptance, before technical editing, formatting and proof reading. Using this free service, authors can make their results available to the community, in citable form, before we publish the edited article. This *Accepted Manuscript* will be replaced by the edited, formatted and paginated article as soon as this is available.

You can find more information about *Accepted Manuscripts* in the [Information for Authors](#).

Please note that technical editing may introduce minor changes to the text and/or graphics, which may alter content. The journal's standard [Terms & Conditions](#) and the [Ethical guidelines](#) still apply. In no event shall the Royal Society of Chemistry be held responsible for any errors or omissions in this *Accepted Manuscript* or any consequences arising from the use of any information it contains.

Cite this: DOI: 10.1039/c0xx00000x

www.rsc.org/xxxxxx

ARTICLE TYPE

Facile and green synthesis of graphene oxide by electrical exfoliation of pencil graphite and gold nanoparticle for non-enzymatic simultaneous sensing of ascorbic acid, dopamine and uric acid

Habibulla Imran, Palinci Nagarajan Mainkandan, Venkataraman Dharuman*

Received (in XXX, XXX) Xth XXXXXXXXXX 20XX, Accepted Xth XXXXXXXXXX 20XX

DOI: 10.1039/b000000x

Abstract

Pencil graphite is electrochemically exfoliated to obtain few layered graphene oxide (GO) in hydrochloric acid (HCl, HGO), sodium hydroxide (NaOH, NGO) and phosphate buffer saline (PBS, pH 7.4, PGO) media at a constant potential (+7.0 V) without ionic liquid for the first time. Thus, obtained graphene oxide is deposited (by drop casting and electro reduction) onto a glassy carbon electrode (GCE). Following this, gold nanoparticles (AuNP) are electro deposited to form GO-AuNP composite for simultaneous discrimination of dopamine (DA), ascorbic acid (AA) and uric acid (UA) at pH 7.4. Cyclic voltammetry (CV) and differential pulse voltammetry (DPV) techniques reveal well separated oxidation peaks for DA, AA and UA. The sensor surfaces are characterized by Ultraviolet Visible (UV-Vis), Photoluminescence (PL), X-ray diffraction (XRD), Fourier transform Infrared (FTIR), contact angle goniometry (CA) and scanning electron microscopy (SEM) techniques. DA, AA and UA are studied individually to evaluate the dynamic ranges and lowest detection limits of the sensor by the DPV method. Concentrations of DA, AA and UA in real samples viz., dopamine injection, vitamin C tablets and human urine samples are evaluated.

1. Introduction

Neuro transmitters dopamine (DA), ascorbic acid (AA) and uric acid (UA) co-exist in biological sample and change in their concentration levels beyond the critical limits (above micro molar concentration) lead several health disorders. For instance, while variation in dopamine concentration affects brain function and induces neurological disorders like Parkinson's disease and drug addiction¹⁻⁴, the abnormal levels of uric acid (UA) regulates gout and hyperuricemia^{5,6} and change in AA concentration induces skin and immune system⁷. Since these substrates regulate different diseases and are interrelated to each other, simultaneous detection of concentration levels of DA, UA and AA is of high interest in biomedical chemistry, neurochemistry, diagnostic and pathological investigations. Although various techniques including liquid chromatography⁸, mass spectrometry⁹ spectrophotometry¹⁰ and electrochemical¹¹⁻¹³ are used for sensitive and selective detection, the electrochemical method is extensively investigated for its simplicity, cost-effectiveness and

Molecular Electronics Laboratory, Department of Bioelectronics and Biosensors, Science Campus, Alagappa University, Karaikudi – 630 004 India.

*To whom correspondence should be addressed. V. Dharuman, E-mail: dharumanudhay@yahoo.com Phone: 91-4565-223361 Fax: 91-4565-225525

Electronic Supplementary Informations FTIR, UV, contact angle measurement, C and DPV are available at see DOI: 10.1039/b000000x

user friendliness¹⁴⁻¹⁶. However, most of the reported sensors focus on the single analyte detection of either DA or AA for two reasons. (i) All these three analytes have similar oxidation potentials and sensor signals overlap each other¹⁴⁻¹⁶. (ii) The DA poisons the surface by its adsorption on carbon surface. Therefore, during the last five decades, intense research is directed to the development of sensitive electrodes for lower concentrations (0.01 to 1 μM) of DA in presence of 100 to 1000 fold excess of AA and UA.

Currently, graphene with metal/polymer composites are being applied in nanoelectronics, sensors, nanocomposites, batteries and super capacitors due to the increase in its intrinsic properties like electrical, thermal conductivity¹⁷, optical¹⁸, specific surface area¹⁹, biocompatibility^{20,21}, mechanical strength and transparency²². Metal²³, metal oxides^{24,25}, carbon nano structures²⁶⁻²⁸ and polymers^{16, 29, 30} decorated graphene are reported for simultaneous determination of AA, DA and UA³¹⁻³⁴. Graphene is prepared by different routes such as thermal decomposition on SiC wafer under ultrahigh vacuum (UHV)³⁵⁻³⁸, CVD growth on metal substrates (ruthenium³⁹, Ni^{39, 40}, and Cu⁴¹) substrate free CVD⁴², chemical⁴³⁻⁴⁷ and thermal reduction⁴⁸ of graphite in different studies. While mechanical exfoliation⁵⁰, thermal decomposition⁵¹, oxidation of graphite⁵² and liquid-phase exfoliation of graphite^{53,54} from single or few-layer graphene, the electro reduction^{55,56} produces thick layered graphenes. Surfactants, polymers and metal nanoparticles⁵⁷⁻⁶⁰ are suggested to avoid the restacking. Since, the AuNP is more biocompatible and has tunable electronic properties, Li *et. al.*^{61,62} have developed graphene-AuNP for the selective determination of DA

with a detection limit of 1.86 μM . One-step solvothermal synthesis of graphene-AuNP composite is reported for simultaneous detection of DA, AA and UA^{63, 64}. Although electrochemical exfoliation of graphite in presence of ionic liquid is reported,⁶⁵ avoiding the toxic and expansive chemicals and simplifying the product recovery processes is essential. In this regard, electrical exfoliation in NaOH is recently reported, but used H_2O_2 for GO reduction⁶⁶ and not applied for any neurotransmitter detection. Therefore, this study aims to exploit the exfoliation of graphene in aqueous medium as there is no report available on the use of electrochemically exfoliated graphene oxide and gold nanoparticle composite till now for simultaneous sensing of DA, AA and UA. The graphene oxide is prepared by the electric exfoliation of pencil graphite in hydrochloric acid, phosphate buffer and sodium hydroxide without using any ionic liquid or metal/metal oxide to prevent aggregation/restacking of graphene oxides. Thus obtained GO is deposited on the glassy carbon electrode surface by two different methods viz., drop casting and electrochemical reduction of GO on the GCE. This is followed by gold nanoparticles deposition by electro reduction of $\text{HAuCl}_4 \cdot 3\text{H}_2\text{O}$. Simultaneous detection of DA, AA and UA is made with and without gold nanoparticle decoration and compared.

2. Experimental section

2.1. Materials and methods

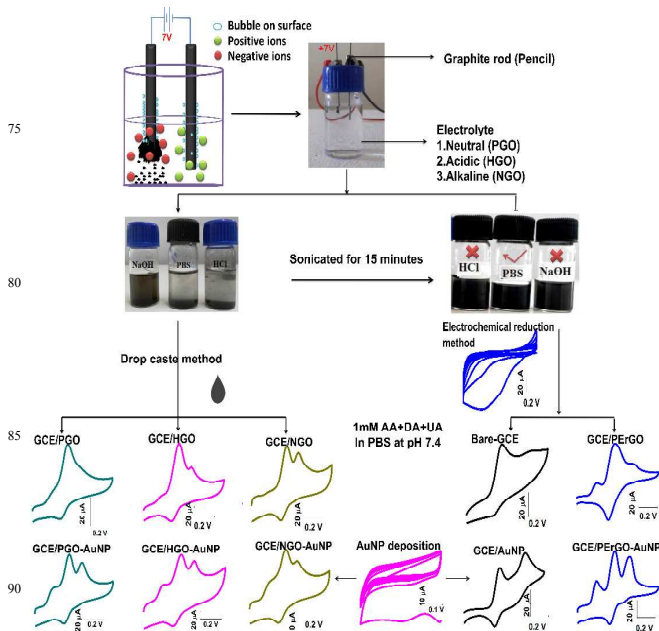
Pencil used as graphite rod (0.7 mm diameter and 60 mm length, purchased from a stationary shop). Potassium ferrocyanide, potassium ferricyanide, sulfuric acid, sodium chloride, dimethylformamide (DMF), sodium dihydrogen phosphate and potassium chloride of analytical grade were purchased from Himedia, India. Tetrachloroaurate was purchased from Sigma Aldrich, USA. Analytical grade, dopamine, uric acid and ascorbic acid were all purchased from Sisco Research Laboratories Chemicals Pvt. Ltd. India. Milli-Q water (18.2 M Ω) was used for all experiments. 0.01 M phosphate buffer of pH 7.4 containing NaCl (120 mM), NaH_2PO_4 (10 mM) and KCl (2.7 mM) was prepared and used for all electrochemical experiments.

pH Meter from Susima, AP-1PLVS, India, was used for in measuring the solution pH. The electrochemical experiments cyclic voltammetry (CV), chronoamperometry (CA) and differential pulse voltammetry (DPV) were carried out using the CHI 440B electrochemical analyzer/workstation (CH Instruments, USA). A conventional three-electrode system consisting of a glassy carbon working (3 mm diameter), a platinum wire (1 mm diameter and 2 cm long) counter and Ag/AgCl reference electrodes was used. PANalytical make Bruker D8-Advance powder diffractometer which uses $\text{Cu-K}\alpha 1$ radiation (2.2 kW max) was used for powder X-ray diffraction measurements (PANalytical B.V., Lelyweg 1, 7602 EA ALMELO, The Netherlands). Chemical Vapor Deposited gold (100 nm) Si and graphite substrates were used for acquiring the FE-SEM images and EDS spectra using Zeiss SEM instrument which uses a LEO 1530 field emission from Hitachi (model S-3000H), Japan. Images were recorded at an accelerating voltage 10 kV with a secondary electron detector. Homemade variable DC power supply with Digital electronic multimeter was

used to electrochemical exfoliation. UV spectra were recorded using Shimadzu UV2450 high-performance single monochromator instrument in the frequency range 400–700 nm. The contact angle equipment was purchased from AST Products Inc., USA, having an automated model of VCA Optima XE.

2.2. Electrochemical exfoliation of pencil graphite

Graphene oxide was prepared from pencil rod electrochemically by applying a constant DC potential +7 V between two pencil electrodes in an aqueous solution without any ionic liquids. Scheme 1.



Scheme 1: Electrochemical exfoliation of pencil to form graphene oxide and its anchoring on glassy carbon electrode by drop casting (left) and electro reduction (right) followed by gold nanoparticle deposition for simultaneous sensing of dopamine (DA), ascorbic acid (AA) and Uric acid (UA).

Three different aqueous media viz., hydrochloric acid (HCl, named as HGO), phosphate buffer saline (PBS, pH 7.4, named as PGO), and sodium hydroxide (NaOH, named as NGO) were used for exfoliation. The exfoliation takes place at the positive terminal and graphene oxides were formed as flakes. Exfoliation process was completed at different electrolysis time scale depending on the media used and formation of different amount of graphene oxide. For instance, the quantity of graphene oxide formed are 760 $\mu\text{gA}^{-1}\text{s}^{-1}$, 33.6 $\mu\text{gA}^{-1}\text{s}^{-1}$ and 667 $\mu\text{gA}^{-1}\text{s}^{-1}$ respectively in HCl, NaOH and PBS media. The exfoliation rate in different media follows the order HCl (4 minutes with 107 mA) > PBS (11 minutes with 27 mA) > NaOH (45 minutes with 146 mA) for 3 mg of graphite rod exfoliation at +7.0 V. The exfoliated graphene oxide (GO) solution was sonicated for 15 minutes to obtain uniform dispersion of the GO followed by successive washing with double distilled water, ethanol, acetone and filtration by centrifuging at 8000 rpm for 5 minutes. The final product was dried at 45 $^{\circ}\text{C}$ for 2 hours. The product was used for

electrochemical and other characterization by XRD, UV-Vis, FTIR and SEM techniques.

2.4. Fabrication of GO-AuNP modified glassy carbon electrode

For GCE surface modification by drop casting method, 1.5 mg of GO, obtained from pencil graphite exfoliation, was dispersed in 1 mL of DMF followed by sonication for 1 hour. 2 μ L of the mixture is drop casted on the GCE and dried at an ambient temperature for 30 minutes. The AuNP was then deposited by electro reduction of $\text{HAuCl}_4 \cdot n\text{H}_2\text{O}$ by potential cycling in the window 0 to -0.6 V for 20 cycles. For electrochemical modification of GO on the GCE, 3 mg of GO in 5 mL of PBS was taken and potential cycled in the window 0 to -1.6 V for 20 cycles. This step again followed by the AuNP deposition similar to that of drop casting method.

3. Results and Discussion

3.4. Characterization of exfoliated graphene oxide

The CV curves of the GCE modified using the PGO, HGO and NGO by the drop casting method are recorded in presence of $[\text{Fe}(\text{CN})_6]^{3-/4-}$ redox probe in PBS (pH 7.4), Fig. 1. All composites show increased peak currents compared to the unmodified GCE, however, differences exists between their CV profiles.

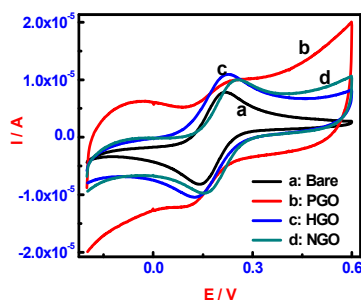


Fig. 1. CV behaviors of GCE (curve a) modified using graphene oxide obtained by the electrical exfoliation of pencil graphite in PBS (curve b), HCl (curve c), and NaOH (curve d). The GO is dispersed in DMF and drop casted on the GCE and dried at ambient temperature. Measurements are made in presence of $[\text{Fe}(\text{CN})_6]^{3-/4-}$ in PBS (pH 7.4) at a scan rate 50 mVs^{-1} .

For instance, the GCE-PGO showed diffused peaks with very low peak currents, while the GCE-HGO and GCE-NGO showed sharp and reversible peaks. Generally, the charge transfer from the $[\text{Fe}(\text{CN})_6]^{3-/4-}$ to the GO modified surface decreases due to electrostatic repulsion from the intrinsic functional groups (epoxide, acid, hydroxyl) of GO and $[\text{Fe}(\text{CN})_6]^{3-/4-}$. Hence, increased charge transfer in the presence of $[\text{Fe}(\text{CN})_6]^{3-/4-}$ for the GCE-HGO and GCE-NGO indicates the formation of GO with less functional groups. Nature of these graphene oxides are further characterized by the UV. The UV shows two peaks at ~ 227 (arising from $\pi-\pi^*$ transition of the atomic C-C bonds) and ~ 250 nm ($n-\pi^*$ transitions of aromatic C-C bonds²⁷), respectively, suggesting the introduction of oxygen functional groups, Fig. S1. More interestingly, while the NGO

and HGO show only two absorption peaks (220 and 250 nm), the PGO shows three absorption peaks at 220, 250 and 314 nm, respectively, indicating higher conjugation of pi electron network in the PGO than in the other two composites⁶⁷. All samples exhibited predominantly D and G bands^{29,32-33} at 1300 and 1500 cm^{-1} , respectively, in Raman spectra. Both the D and G bands arise from the double resonance effects at graphene defects. Both bands are blue shifted by 10 cm^{-1} with week intensities for the HGO indicating high exfoliation of graphite in HCl medium.

Methods of graphene oxide or graphene preparation have significant effects on the positions of the D, G and 2D bands in the Raman spectra, Fig.2A, similar to that reported for a few-layer graphenes prepared by epitaxial growth on SiC, which shows a blue shifted G-band (ca. 20 cm^{-1}) and 2D bands (ca. 60 cm^{-1}) compared to the exfoliated graphene⁶⁶. Shifts in the position of Raman bands of three different GO indicate significant effect of the medium used for the exfoliation. The graphenization is very high in NaOH than in the HCl and PBS. The ratio of I_D/I_G expresses the sp^2/sp^3 carbon ratio manifesting on the measure of disorder³⁴ at the edges, charge distribution and wrinkle nature. Highest ratio of I_D/I_G (1.12) is observed for the PGO compared to the HGO (0.984) and NGO (0.314) suggests the introduction of oxygen functionality that increased the disordered corner edges in the PGO. These observations indicate the fact that more graphite flakes formed in HCl and NaOH. Photoluminescence shows a triplet peak for these graphene sheets, Fig.S2. Among these three, the PGO showed maximum PL emission indicating the highest carrier – carrier scattering over the electron phonon scattering. It may be noted that the shape of the PL spectra highly dependent on the size and shape of the quantum sized carbon networks⁶⁸.

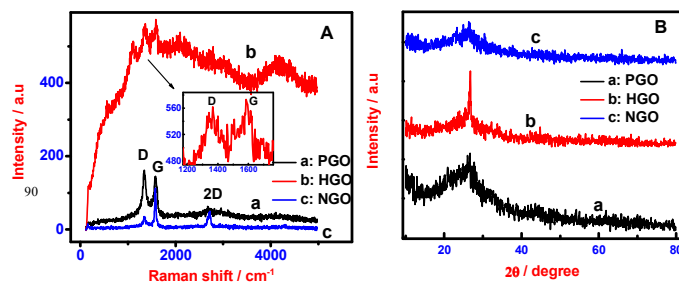


Fig. 2. Raman spectra (A) and XRD patterns (B) of PGO (curve a), HGO (curve b) and NGO (curve c).

The X-ray diffraction patterns of the PGO, HGO and NGO are presented in Fig. 2B. The broadening of Bragg's peak indicates the formation of crystalline graphene whose size is calculated using the Scherer formula $D = K\lambda/\beta_s \cos\theta$, where D is the average size of the crystal, K is the shape dependent Scherer's constant, λ is the wavelength of radiation, β_s is the full peak width at half maximum and θ is the diffraction angle³⁶. Using the full width half maxima (FWHM) of (111) peak, crystal sizes of the PGO, HGO and NGO calculated are 1.4, 21 and 2.3 nm. The crystal size calculated from I_D/I_G ratio using the formula $L_a = 2.4 \times 10^{-10} \lambda^4 [I_D/I_G]^{-1}$ are 3.8, 4.1 and 0.7 nm respectively. SEM images of the PGO, HGO and NGO are presented in Fig.3. Highly disintegrated sheets formed in HCl medium whereas smooth sheets are obtained in NaOH. The sheets prepared in PBS appears little rougher than that obtained in NaOH. That is, the I_D/I_G ratio values observed are well corroborates the SEM

morphological features. The highest I_D/I_G ratio, smaller crystal size (from XRD measurements), and maximum PL peak intensity observed for the PGO suggest the more hydrophilic nature of the PGO than the NGO(80.2°) and HGO (92.3°) and confirmed by the highest contact angle of 108.9°, Fig. S3.

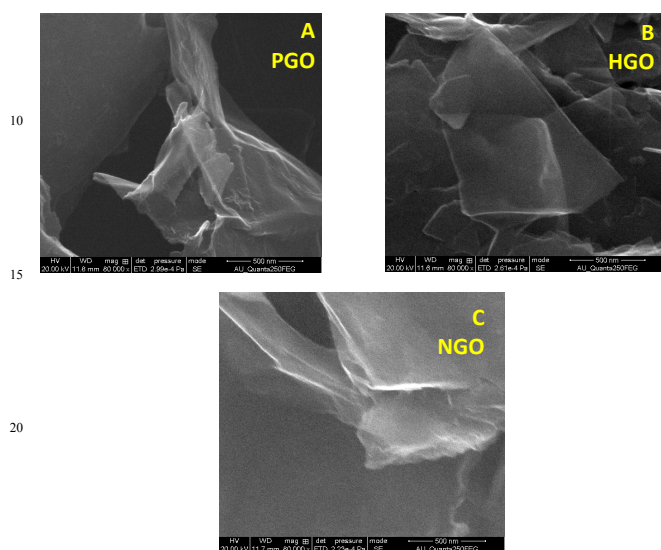


Fig. 3. SEM images of GO obtained from electrical exfoliation of graphite in (A) HCl; (B) Phosphate buffer pH 7.4 and (C) NaOH.

The PGO is used to modify the GCE and tested for simultaneous detection of the DA, UA and AA. Although multiple peaks are obtained, the peaks are not well separated on the GO. Only a single reversible peak corresponding to DA in the potential region 0 to 0.3 V is observed, Fig.4A, Curve a.

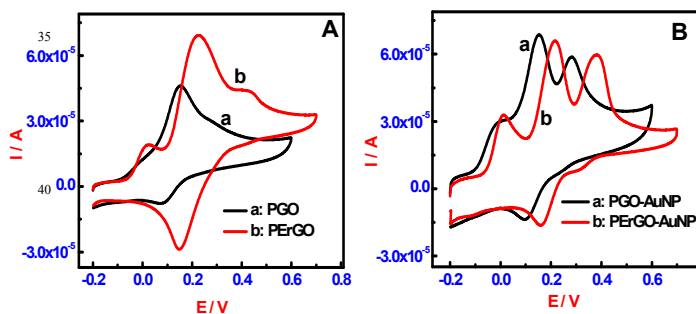


Fig. 4 Simultaneous detection of 1mM concentrations of ascorbic acid, uric acid and dopamine in PBS (pH 7.4). In the absence (A) and presence (B) of AuNP on the PGO (curve a) and PErGO (curve b) modified GCEs.

3.5. Behavior of electrochemically deposited ErGO in presence of $[Fe(CN)_6]^{3-/4-}$

Since the method of surface preparation influences greatly the detection of target analytes, in this work, graphene is deposited by electrochemically reducing the PGO in the potential window 0 to -0.18 V (75 cycles) in phosphate buffer to modify the GCE surface with ErGO and named as GCE-PErGO.

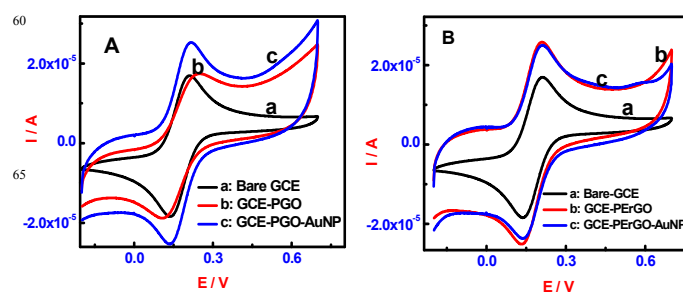


Fig. 5. CV behaviors of GCE (curve a), (A) the GCE modified by PGO by drop casting (curve b) and followed by electrochemically deposited AuNP (curve c), (B) CV behaviors of GCE (curve a) modified by the electrochemical reduction of PGO (PErGO) by potential cycling (curve b) followed by electrochemically deposited AuNP (curve c). Measurements are made in presence of 1mM $[Fe(CN)_6]^{3-/4-}$ in PBS (pH 7.4) at a scan rate 50 mVs⁻¹.

Fig. 5A depicts the comparative CV profiles of the GCE modified using the PGO (drop casted, curve b) and PGO-AuNP (curve c) measured in presence of $[Fe(CN)_6]^{3-/4-}$. The peak currents decrease due to electrostatic repulsion from the intrinsic functional groups in the prepared GO. Upon deposition of AuNP, the peak currents increase nearly equivalent to the unmodified GCE because of electrocatalysis. Similarly, Fig.5B presents the CV behaviors of the GCE (curve a) modified by electro reduction of GO by the potential cycling to form GCE-PErGO (curve b) and GCE-PErGO-AuNP (curve c). It may be noted that the current for the GCE-PErGO is increased by 50 % compared to the CV profile of the GCE-PGO, indicating the reduction of functional groups on the PGO electrochemically.⁶⁷ Application of the GCE-PErGO for the simultaneous detection of AA, DA and UA showed a larger reversible peak for the DA which is flanked by the small and irreversible peaks for the AA and UA, Fig.4A, curve b. Recently, metal nanoparticle-graphene composites show a promising performance in the field of biosensors, however, methods of preparation origin again proved to influence the sensor performance.⁶⁸ It is to note that the peak currents magnitude for GCE-PGO-AuNP and GCE-PErGO-AuNP are nearly same. No significant changes in the CV profiles of these two modified GCEs are observed. This is attributed to the even deposition of gold nanoparticles on both the GCE-PGO and GCE-PErGO. This is possible because the GCE-PGO surface is prepared by the drop casting method which uses volatile DMF solvent and the exposed PGOs are encapsulated by the AuNPs. The similar process also applicable to the GCE-PErGO surface as well and hence, only AuNP are in contact with the $[Fe(CN)_6]^{3-/4-}$ for charge transfer resulting in similar CV behaviors. The SEM images of the PGO, PErGO and PErGO-AuNP are presented in Fig.6. The electro reduction of PGO (Fig. 6A) results in the formation of clear, silky, wrinkled granules of PErGO (Fig. 6B) and the AuNP are evenly deposited on the PErGO (Fig. 6C).

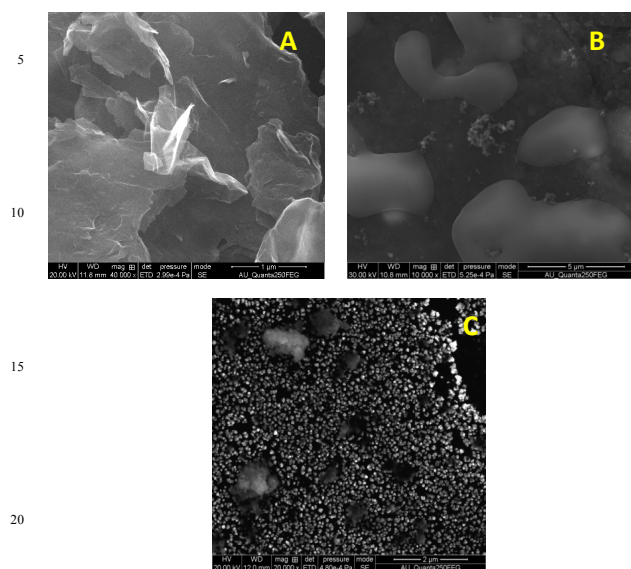


Fig. 6. SEM images of PGO (A), PErGO (B) and PErGO-AuNP (C) films

Both the PGO-AuNP and PErGO-AuNP modified GCEs are tested for the simultaneous detection of AA, DA and UA. The peaks are well separated on both the GO-AuNP surfaces, however, significant differences are clear between the two CV profiles, Fig.4B. The GCE-PErGO-AuNP surface exhibits well defined peaks for all these analytes in CV. The CV peak current increases for the AA and UA, whereas it decreases for the DA. While AA peak potential remains the same at 0.01V on both the GCE-PGO-AuNP and GCE-PErGO-AuNP, the peak potentials for the DA and UA on the GCE-PErGO are shifted positively by ~0.1V. The positive shifts of peak potentials for the DA and UA are attributed to the oxidation products of these compounds on the PErGO-AuNP and repulsion of π electrons on the reduced GO and aromatic π electrons in the DA and UA. The presence of AuNP suppresses the capacitive current observed for the GCE-PGO-AuNP in the potential region where the target analytes are reacting. In order to study the effect of concentration of each analyte individually, more sensitive DPV technique is used.

3.3 Effect of analyte concentrations

Effect of target analyte concentration is studied using both the GCE-PGO-AuNP (Fig.S4) and GCE-PErGO-AuNP (Fig. 7A-C) by varying the concentration of one analyte while the concentrations of other two analytes kept constant. When the GCE-PGO-AuNP surface is used, the charging current in the potential region where the non-sensing analytes (concentrations kept constant) increases with increasing the concentration of target analyte of interest. In contrast, on the GCE-PErGO-AuNP the charging current remains unaltered when the concentration of target analyte of interest is increased. Hence, for further analysis, the GCE-PErGO-AuNP is used. Direct proportionality between the analyte concentration and current signal is noticed over a wide concentration range studied, 1nM to 5000 μ M. The linear relationships are given by the following equations.

$$i = 0.0144 \text{ AM}^{-1} \times [\text{AA}] + 3.92 \times 10^{-6} \text{ A} \quad || \quad (r^2 = 0.995) \text{-----(1)}$$

$$i = 0.0253 \text{ AM}^{-1} \times [\text{UA}] + 2.77 \times 10^{-6} \text{ A} \quad || \quad (r^2 = 0.994) \text{-----(2)}$$

$$60 \quad i = 0.0412 \text{ AM}^{-1} \times [\text{DA}] + 7.83 \times 10^{-6} \text{ A} \quad || \quad (r^2 = 0.985) \text{-----(3)}$$

It is observed from the literature survey on the enzymatic detection of dopamine⁷⁰ that the detection limit and sensitivity are significantly depend on the procedure used for the immobilization matrix. Michaelis–Menten (MM) kinetic parameters K_M , V_{max} , and k_{cat} reveal the influences of the physical and chemical properties of the surface on the efficiency of the catalytic reactions. Michaelis–Menten (MM) constant, K_M , is defined as the substrate concentration up to which the current increases linearly, V_{max} is the maximum rate of the enzymatic reaction and k_{cat} is the turnover number of the enzyme. Since the GO-AuNP composite behaves similar to enzyme, the MM kinetics is applied to evaluate the parameter, K_M . Respective Lineweaver-Burk plots for the GCE-PGO-AuNP and GCE-PErGO-AuNP are shown in Fig. S5. From the intercepts and slopes of Fig.S5, the calculated K_M values are listed in Table S1. For the DA detection observed K_M are 0.07 and 110 mM, respectively, at the GCE-PGO-AuNP and GCE-PErGO-AuNP surfaces. The higher K_M observed for the GCE-PErGO-AuNP suggests enhanced diffusion restriction property resulting from the electrostatic repulsions between the π electrons in the PErGO and dopamine π electrons. A similar observation is also made for AA and UA as noticed from the K_M values, Table S1. From the equations 1-3, higher sensitivity of $0.0412 \text{ AM}^{-1} \text{ L}^{-1}$ is obtained for DA than that of the AA and UA. Hence, the GCE-PErGO-AuNP sensor is more selective for the DA than the AA and UA. Further, the GCE-PGO-AuNP showed quick saturation at concentrations below 10 mM for DA, Fig. S4B. The lowest detection limits and the dynamic ranges are given in Table S1 and comparison with the literature reports is given in Table S2. It is to note that the GCE-PErGO-AuNP show wide linear range, lowest detection limit than the literature reports. Fig.S6 presents the reproducibility of the AA, DA and UA at the GCE-PErGO-AuNP surface. It noted that the observed relative standard deviation (RSD) for four time repetition of the AA (0.11), DA (0.17) and UA (0.12) detections suggests the high reproducibility and stability of this sensor device.

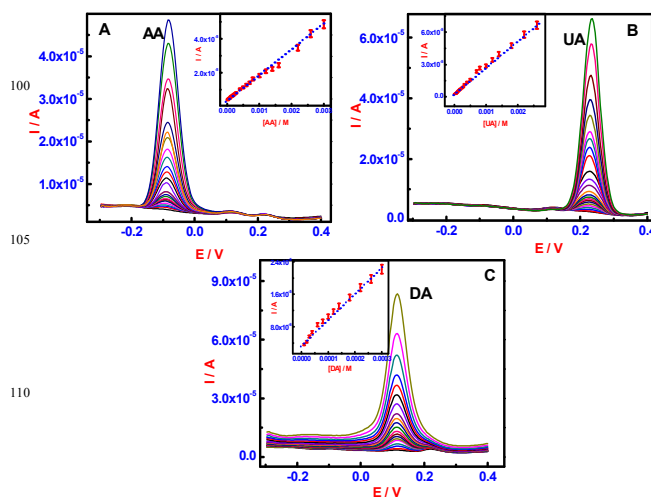


Fig. 7. Selective detection of various concentrations of ascorbic acid (A), uric acid (B) and dopamine (C) at GCE-PErGO-AuNP in phosphate buffer by DPV measurement in presence of excess concentration of other analytes. Inset: Current versus concentration plots of the respective

3.4 Real sample analysis

The GCE-PErGO-AuNP surface is then used for analysing the content of AA in amla juice, vitamin C tablet (obtained from medical shops in our region), UA in urine and DA in commercial dopamine hydrochloride injections (purchased from medical shops in our region) using simple linear sweep voltammetry (LSV). Fig. 8A compares the sensor response for the commercially obtained AA (1 mM, curve b) with concentrations of AA in the real samples such as Vitamin C tablet (curve c) and Amla juice (curve d). For this, 0.8 mg (1 mM) of vitamin C tablet is dissolved in 5 ml. 500 μ L of amla juice is diluted in 5 ml PBS. It is evidenced that sensor is well discriminates different concentrations of AA in different commercial samples. Similar experiments were made for the detections of UA (Fig. 8B) in urine and DA (Fig. 8C) in commercial dopamine injection. The sensor behavior is compared with the clinical data, Fig. 8. From, Fig. 8 B and C, it is evident that the sensor showed nearly equal current signals for both the commercial UA and DA and real samples. In Fig.8A, the AA signal for the vitamin C is slightly decreases, whereas increased signal is noticed for the ascorbic acid in the Amla juice.

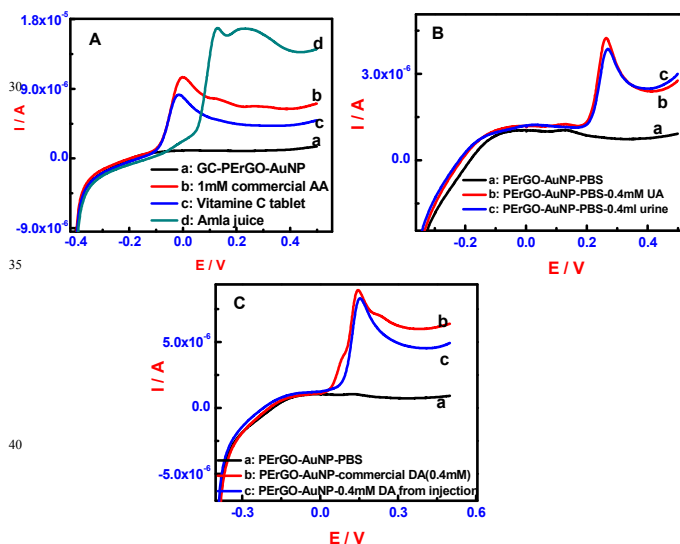


Fig. 8 (A) Comparison of LSV behaviors of the GCE-PErGO-AuNP in PBS buffer (curve a) for detections of ascorbic acid in commercial (curve b), real samples vitamin C (curve c) and amla juice (curve d). (B) Comparative LSV curves for the commercial uric acid (curve b) and uric acid present in urine sample (curve c). (C) Dopamine detection commercial (curve b) and dopamine hydrochloride injection (curve c). LSV is recorded at a scan rate 50 mVs^{-1} .

4. Conclusions

Three media have been tested for electrical exfoliation of pencil graphite to produce graphene cost effectively. Among the three media used, the phosphate buffer with pH 7.4 is the best suited for producing high quality and few layered graphene oxide than the HCl and NaOH. The green synthesis of graphene oxide by

electrical exfoliation and gold nanoparticle by electro-reduction is a simple method to prepare graphene and gold metal composite film. The GCE-PErGO-AuNP exhibit well defined and separated peaks for AA, DA and UA than the GCE-PGO-AuNP. The gold nanoparticle is evenly deposited on both GCE-PGO and GCE-PErGO irrespective of the method of the film formation on the GCE indicating the fact that DMF is a good solvent which is evaporated completely and GO are capped by the AuNPs. Although this is common for both the GCE-PGO-AuNP and GCE-PErGO-AuNP indicated by the similar CV behaviors, the presence of AuNP on the GCE-PErGO eliminates charging current contribution completely in DPV which is essentially required for the developing more sensitive biosensors for other biotechnological applications well. The lowest detection limit for dopamine observed is 10 nM with the linear range of 10 nM to 3000 μ M.

Acknowledgement

The authors acknowledge the Department of Industrial Chemistry and the Department of Physics, Alagappa University for providing material characterization facilities. The authors acknowledge University Grants Commission India for financial support. P. N. Manikandan acknowledge the Department of Science and Technology of India for award INSPIRE Fellowship (IF 140744).

References

- [1] J. Ping, J. Wu, Y. Wang, Y. Ying, *Biosensors Bioelectronics*, 2012, **34**, 70
- [2] A. Ciszewski, G. Milczarek, *Analytical Chemistry*, 1999, **71**, 1055.
- [3] A. Salimi, K. Abdi, GR. Khayatian, *Microchimica Acta*, 2004, **144**, 161
- [4] Y. Zhao, Y. Gao, D. Zhan, H. Liu, Q. Zhao, Y. Kou, Y. Shao, M. Li, Q. Zhuang, Z. Zhu, *Talanta*, 2005, **66**, 51
- [5] A. Ensafi, M. Taei, T. Khayamian, A. Arabzadeh, *Sensors Actuators B*, 2010, **147**, 213
- [6] M. Mallesha, R. Manjunatha, C. Nethravathi, G.S. Suresh, M. Rajamathi, J.S. Melo, T. V. Venkatesha, *Bioelectrochemistry*, 2011, **81**, 104.
- [7] U. Yogeswaran, S. Thiagarajan, S. M. Chen, *Analytical Biochemistry* 2007, **365**, 122.
- [8] A. Asan, I. Isildak *Journal of Chromatography A*, 2003, **988**, 145.
- [9] S. C. Moldoveanu, M. Kiser, *Journal of Chromatography A*, 2007, **1141**, 90.
- [10] M.J. Schoning, M. Jacobs, A. Muck, D. T. Knobbe, J. Wang, M. Chatrathi, S. Spillmann, *Sensors and Actuators B Chemical*. 2005, **108**, 688.
- [11] S. R. Ali, P. R. Parajuli, Y. Balogun, Y. F. Ma, H. X. He, *Sensors*, 2008, **8**, 8423
- [12] D. Lakshmi, M. J. Whitcombe, F. Davis, P. S. Sharma, B. B. Prasad, *Electroanalysis*, 2011, **23**, 305
- [13] A. Malinauskas, R. Garjonyte, R. Mazeikiene, I. Jureviciute, *Talanta*, 2004, **64**, 121.
- [14] P. Ramesh, S. Sampath, *Electroanalysis*, 2004, **16**, 866.
- [15] X. H. Lin, Y. F. Zhang, W. Chen, P. Wu, *Sensors and Actuators B* 2007, **122**, 309.
- [16] A. A. Ensafi, M. Taei, T. Khayamian, *Journal of Electroanalytical Chemistry*, 2009, **633**, 212.
- [17] C. Lee, X. D. Wei, J. W. Kysar, J. Hone, *Science*, 2008, **321**, 385
- [18] P. R. Nair, P. Blake, A. N. Grigorenko, K. S. Novoselov, T. J. Booth, T. Stauber, N. M. R. Peres, A. K. Geim, *Science*, 2008, **320**, 1308
- [19] M. D. Stoller, S. J. Park, Y. W. Zhu, J. H. An, R. S. Ruoff, *Nano Letters*, 2008, **8**, 3498
- [20] N. Mohanty, V. Berry, *Nano Letters*, 2008, **8**, 4469
- [21] P. Wu, Q. Shao, Y. Hu, J. Jin, Y. Yin, H. Zhang, C. Cai,

- Electrochimica Acta*, 2010, **55**, 8606
- [22] C. Zhu, S. Dong, *Nanoscale*, 2013, **5**, 1753
- [23] S. Thiagarajan, S. M. Chen, *Talanta* 2007, **74**, 212.
- [24] C. F. Tang, S. A. Kumar, S. M. Chen, *Analytical Biochemistry*, 2008, **380**, 174.
- [25] G. Wang, J. Sun, W. Zhang, S. F. Jiao, B. Fang, *Microchimica Acta*, 2009, **164**, 357.
- [26] Y. Z. Zhang, Y. Pan, S. Su, L. Zhang, S. P. Li, M. W. Shao, *Electroanalysis*, 2007, **19**, 1695.
- [27] K. S. Prasad, G. Muthuraman, J. Zen, *Electrochemical Communications*, 2008, **10**, 559.
- [28] Y. Liu, J. S. Huang, H. Q. Hou, T. Y. You, *Electrochemical Communications*, 2008, **10**, 1431.
- [29] J. H. Chen, J. Zhang, X. H. Lin, H. Y. Wan, S. Zhang, *Electroanalysis*, 2007, **19**, 612.
- [30] H. Yao, Y. Y. Sun, X. H. Lin, Y. H. Tang, L. Y. Huang, *Electrochimica Acta*, 2007, **52**, 6165.
- [31] R. Aguilar, M. M. Da'vila, M. P. Elizalde, J. Mattusch, R. Wennrich, *Electrochimica Acta*, 2004, **49**, 851.
- [32] A. H. Liu, I. Honma, H. S. Zhou, *Biosensors and Bioelectronics*, 2007, **23**, 74.
- [33] J. S. Huang, Y. Liu, H. Q. Hou, Tianyan You, *Biosensors and Bioelectronics*, 2008, **24**, 632.
- [34] D. Zheng, J. S. Ye, L. Zhou, Y. Zhang, C. Z. Yu, (2009) *Journal of Electroanalytical Chemistry*, 2009, **625**, 82.
- [35] W. A. de Heer, C. Berger, X. S. Wu, P. N. First, E. H. Conrad, X. B. Li, T. B. Li, M. Sprinkle, J. Hass, M. L. Sadowski, M. Potemski, G. Martinez, *Solid State Communications*, 2007, **143**, 92.
- [36] K. V. Emtsev, A. Bostwick, K. Horn, J. Jobst, G. L. Kellogg, L. Ley, J. L. McChesney, T. Ohta, S. A. Reshanov, J. Rohrl, E. Rotenberg, A. K. Schmid, D. Waldmann, H. B. Weber, T. Seyller, *Nature Materials*, 2009, **8**, 203.
- [37] E. Rolling, G. H. Gweon, S. Y. Zhou, B. S. Mun, J. L. McChesney, B. S. Hussain, A. Fedorov, P. N. First, W. A. de Heer, A. Lanzara, *Journal of Physics and Chemistry of Solids*, 2006, **67**, 2172
- [38] C. Berger, Z. M. Song, X. B. Li, X. S. Wu, N. Brown, C. Naud, D. Mayo, T. B. Li, J. Hass, A. N. Marchenkov, E. H. Conrad, P. N. First, W. A. de Heer, *Science*, 2006, **312**, 1191.
- [39] P. W. Sutter, J. I. Flege, E. A. Sutter, *Nature Materials*, 2008, **7**, 406.
- [39] K. S. Kim, Y. Zhao, H. Jang, S. Y. Lee, J. M. Kim, J. H. Ahn, P. Kim, J. Y. Choi, B. H. Hong, *Nature*, 2009, **457**, 706.
- [40] A. Reina, X. T. Jia, J. Ho, D. Nezich, H. B. Son, V. Bulovic, M. S. Dresselhaus, J. Kong, *Nano Letters*, 2009, **9**, 30.
- [41] X. S. Li, W. W. Cai, J. H. An, S. Kim, J. Nah, D. X. Yang, R. Piner, A. Velamakanni, I. Jung, E. Tutuc, S. K. Banerjee, L. Colombo, R. S. Ruoff, *Science*, 2009, **324**, 1312.
- [42] A. Dato, V. Radmilovic, Z. H. Lee, J. Phillips, M. Frenklach, *Nano Letters*, 2008, **8**, 2012.
- [43] A. N. Obraztsov, *Nature Nanotechnology*, 2009, **4**, 212.
- [44] S. Stankovich, D. A. Dikin, R. D. Piner, K. A. Kohlhaas, A. Kleinhammes, Y. Jia, Y. Wu, S. T. Nguyen, R. S. Ruoff, *Carbon*, 2007, **45**, 1558.
- [45] S. Gilje, S. Han, M. Wang, K. L. Wang, R. B. Kaner, *Nano Letters*, 2007, **7**, 3394.
- [46] D. Li, M. B. Muller, S. Gilje, R. B. Kaner, G. G. Wallace, *Nature Nanotechnology*, 2008, **3**, 101.
- [47] X. B. Fan, W. C. Peng, Y. Li, X. Y. Li, S. L. Wang, G. L. Zhang, F. B. Zhang, *Advanced Materials*, 2008, **20**, 4490.
- [48] H. C. Schniepp, J. L. Li, M. J. McAllister, H. Sai, M. Herrera-Alonso, D. H. Adamson, R. K. Prud'homme, R. Car, D. A. Saville, I. A. Aksay, *Journal of Physical Chemistry B*, 2006, **110**, 8535.
- [47] R. L. McCreery, *Chemical Reviews*, 2008, **108**, 2646.
- [48] C. E. Banks, T. J. Davies, G. G. Wildgoose, R. G. Compton, *Chemical Communications*, 2005, **829**, 3694
- [49] M. Zhou, Y. L. Wang, Y. Zhai, J. Zhai, W. Ren, F. Wang, S. Dong, *Chemistry*, 2009, **15**, 6116
- [50] E. Casero, C. Alonso, L. Vazquez, M. D. Petit-Dominguez, A. M. Parra-Alfambra, M. de la Fuente, P. Merino, S. Álvarez-García, A. de Andrés, F. Pariente E. Lorenzo, *Electroanalysis*, 2013, **25**, 154.
- [50] K.S. Novoselov, A.K. Geim, S.V. Morozov, D.J. Jiang, Y. Zhang, S.V. Dubonos, I. V. Grigorieva, A.A. Firsov, *Science*, 2004, **306**, 666.
- [51] C. Berger, Z. Song, X. Li, X. Wu, N. Brown, C. Naud, D. Mayou, T. Li, J. Hass, A. N. Marchenkov, E. H. Conrad, P. N. First, W. A. de Heer, *Science*, 2006, **312**, 1191
- [52] D. A. Dikin, S. Stankovich, E. J. Zimney, R. D. Piner, G. H. B. Dommett, G. Evmenenko, S. T. Nguyen, R. S. Ruoff, *Nature*, 2007, **448**, 457
- [53] X. L. Li, X. R. Wang, L. Zhang, S. W. Lee, H. J. Dai, *Science*, 2008, **319**, 1229
- [54] X. L. Li, G. Y. Zhang, X. D. Bai, X. M. Sun, X. R. Wang, E. G. Wang, H. J. Dai, *Nature Nanotechnology*, 2008, **3**, 538
- [55] V. C. Tung, M. J. Allen, Y. Yang, R. B. Kaner, *Nature Nanotechnology*, 2008, **4**, 25
- [56] H. C. Schniepp, J. L. Li, M. J. McAllister, H. Sai, M. Herrera-Alonso, D. H. Adamson, R. K. Prud'homme, R. Car, D. A. Saville, I. A. Aksay, *Journal of Physical Chemistry B*, 2006, **110**, 8535
- [57] Y. Qian, C. Y. Wang, Z. G. Le, *Applied Surface Sciences* 2011, **257**, 10758
- [58] M. Fang, K. G. Wang, H. B. Lu, Y. L. Yang, S. Nutt, *Journal of Materials Chemistry*, 2010, **20**, 1982
- [59] H. He, C. Gao, *Chemistry of Materials*, 2010, **22**, 5054
- [60] F. Y. Zhang, Z. H. Wang, Y. Z. Zhang, Z. X. Zheng, C. M. Wang, Y. L. Du, W. C. Ye, *International Journal of Electrochemical Science*, 2012, **7**, 19
- [61] K. Zhou, Y. Zhu, X. Yang, C. Li, *Electroanalysis*, 2010, **22**, 259
- [62] J. Li, J. Yang, Z. Yang, L. Li, Y. Yu, Q. Xu, X. Hu, *Analytical Methods*, 2012, **4**, 1725
- [63] C. Wang, F. Ye, H. Wu, Y. Qian, *International Journal of Electrochemical Science*, 2013, **8**, 2440
- [64] J. Du, R. Yue, F. Ren, Z. Yao, F. Jiang, P. Yang, Y. Du, *Gold Bull*, 2013, **46**, 137
- [65] N. Liu, F. Luo, H. Wu, Y. Liu, C. Zhag, J. Chen, *Advanced Functional Materials*, 2008, **18**, 1518
- [66] K. S. Rao, J. Senthilnathan, Y. F. Liu, M. Yoshimura, *Scientific Reports*, 2013, **4**, 4237
- [68] V. Dharuman, J. H. Hahn, K. Jayakumar, W. Tang, *Electrochimica Acta*, 2013, **114**, 590
- [68] S. Xu, L. Yong, P. Wu, *Journal of American Chemical Society*, 2013, **5**, 654
- [69] S. Kim, S. W. Hwang, M. Kim, D. Y. Shin, D. H. Shin, C. O. Kim, S. B. Yang, J. H. Park, E. Hwang, S. Choi, G. Ko, S. Sim, C. Sone, H. J. Choi, S. Bae, B. H. Hong, *ACS Nano*, 2012, **6**, 8203.
- [70] S. Tembe, M. Karve, S. Inamdar, S. Haram, J. Melo, S. F. D'Souza *Analytical Biochemistry*, 2006, **349**, 72.